Self-Navigated Low-Rank MRI for MPIO-Labeled Immune Cell Imaging of the Heart

Anthony G. Christodoulou[1], Yijen L. Wu[2], T. Kevin Hitchens[2], Chien Ho[2], and Zhi-Pei Liang[1]

***Abstract*— Super-paramagnetic iron oxide (SPIO) particles can magnetically label immune cells in circulation; the accumulation of labeled cells can then be detected by magnetic resonance imaging (MRI). This has enormous potential for imaging inflammatory responses in the heart, but it has been difficult to do *in vivo* using conventional free-breathing, ungated cardiac imaging. Subspace imaging with temporal navigation and sparse sampling of $(\mathbf{k}, t)$-space has previously been used to accelerate several cardiac imaging applications, conventionally alternating between acquiring navigator data and sparse data every other T_{R}. Here we describe a more efficient self-navigated pulse sequence to acquire both navigator and sparse $(\mathbf{k}, t)$-space data in the space of a single T_{R}, doubling imaging speed to approach 100 frames per second (fps). We show the feasibility of using the resulting method to assess myocardial inflammation in a pre-clinical rodent ischemic reperfusion injury (IRI) model using micron-sized paramagnetic iron oxide (MPIO) particles to label immune cells *in situ*.**

I. INTRODUCTION

Immune cell tracking with magnetic resonance imaging (MRI) noninvasively assesses immune responses *in vivo* by detecting the accumulation of magnetically labeled cells, providing a powerful tool for biomedical research, cellular medicine, and diagnosis. Immune cells are involved in many important physiological and pathological conditions in the heart, such as in atherosclerosis, inflammation, coronary heart disease, and organ rejection, among others [1]. However, cardiac and respiratory motion present significant challenges for imaging inflammatory responses in the heart using MRI, a relatively slow imaging modality.

Macrophages and monocytes can be labeled in circulation by direct intravenous injection of biologically compatible super-paramagnetic iron oxide (SPIO) particles; these cells then migrate to the site of injury, infection, or inflammation. The SPIO particles induce local magnetic field inhomogeneity, shortening the T_2^* of the surrounding water, providing a mechanism to generate negative image contrast. However, the late echo time required for T_2^* weighting leads to long pulse sequences and inefficient data acquisition, making the difficult task of free-breathing, ungated cardiac imaging even more challenging. There is a great need for accelerated cardiac imaging methods, particularly those which are specifically designed for T_2^*-weighted imaging.

Explicit-subspace imaging based on the partial separability (PS) model has been a successful approach for accelerating other cardiovascular imaging applications, and shows promise for accelerating labeled-cell imaging in the heart. The PS model expresses the dynamic cardiovascular image $\rho(\mathbf{r}, t)$ as

$$\rho(\mathbf{r}, t) = \sum_{\ell=1}^{L} \psi_\ell(\mathbf{r})\varphi_\ell(t), \tag{1}$$

and the $(\mathbf{k}, t)$-space signal $d(\mathbf{k}, t)$ as

$$d(\mathbf{k}, t) = \int \rho(\mathbf{r}, t) e^{-i2\pi\mathbf{k}\cdot\mathbf{r}}\, d\mathbf{r} = \sum_{\ell=1}^{L} \tilde{\psi}_\ell(\mathbf{k})\varphi_\ell(t), \tag{2}$$

where $\psi_\ell(\mathbf{r})$ and $\varphi_\ell(t)$ are the ℓth spatial coefficient and temporal basis functions, respectively, and $\tilde{\psi}_\ell(\mathbf{k}) = \mathcal{F}_{\mathbf{r}}\{\psi_\ell(\mathbf{r})\}$. This model induces low-rankness of $\mathbf{C}$, the Casorati matrix formed with elements $C_{ij} = d(\mathbf{k}_i, t_j)$ for any sampling points specified by $\{\mathbf{k}_m\}_{m=1}^M$ and $\{t_n\}_{n=1}^N$:

$$\mathbf{C} = \begin{bmatrix} d(\mathbf{k}_1, t_1) & d(\mathbf{k}_1, t_2) & \dots & d(\mathbf{k}_1, t_N) \\ d(\mathbf{k}_2, t_1) & d(\mathbf{k}_2, t_2) & \dots & d(\mathbf{k}_2, t_N) \\ \vdots & \vdots & \ddots & \vdots \\ d(\mathbf{k}_M, t_1) & d(\mathbf{k}_M, t_2) & \dots & d(\mathbf{k}_M, t_N) \end{bmatrix}.$$

It can be shown that $\mathbf{C}$ has rank no more than L [2], [3] and resides in a temporal subspace described by $\mathbf{C}^H \in \mathrm{R}(\mathbf{\Phi}^H)$, where $\mathbf{\Phi}$ can be formed with elements $\Phi_{ij} = \varphi_i(t_j)$. Explicit-subspace PS imaging is characterized by collecting "navigator" data with high temporal resolution to determine $\mathrm{R}(\mathbf{\Phi}^H)$ and collecting sparse entries of $\mathbf{C}$ for reconstruction using the temporal subspace constraint. Past efforts have collected navigator data and sparse data after separate RF pulses, i.e., in the space of at least $2T_{\mathrm{R}}$.

This paper describes a "self-navigated" method which takes advantage of the unused time before the late echo of T_2^*-weighted MRI to collect both navigator data and sparse data in the space of a single T_{R}, doubling the imaging speed of T_2^*-weighted MRI. Section II provides further background on data acquisition and image reconstruction for explicit-subspace imaging, and Section III describes the self-navigation method. Section IV shows an experimental comparison of navigation strategies and a demonstration of *in vivo* micron-sized paramagnetic iron oxide (MPIO)-labeled cell imaging using self-navigated T_2^*-weighted imaging, corroborated by *ex vivo* T_2^*-mapping using MR microscopy (MRM). Section V contains the conclusion.

This work was supported in part by NIH-R01-EB013695, NIH-P41-EB001977, and NIH-P41-EB015904.

A. G. Christodoulou and Z.-P. Liang are with the Department of Electrical and Computer Engineering and Beckman Institute of Advanced Science and Technology, Urbana, IL, 61801 USA (e-mail: christo8@illinois.edu).

Y. L. Wu, T. K. Hitchens, and C. Ho are with the Pittsburgh NMR Center for Biomedical Research, Department of Biological Sciences, Carnegie Mellon University, 4400 Fifth Avenue, Pittsburgh, PA 15213.

978-1-4244-7929-0/14/$26.00 ©2014 IEEE

II. BACKGROUND

Explicit-subspace low-rank imaging often collects two sets of $(\mathbf{k}, t)$-space data. The navigator data set $\mathcal{D}_1$ covers limited $\mathbf{k}$-space locations at a high temporal rate, enabling high temporal resolution: the frame rate of the final images is equal to the temporal sampling rate of $\mathcal{D}_1$. These data are used to determine the temporal subspace $\mathrm{R}(\mathbf{\Phi}^H)$, so they need not share contrast weighting with the desired image $\rho(\mathbf{r}, t)$. The imaging data set $\mathcal{D}_2$, which determines the contrast weighting, sparsely covers the remainder of $(\mathbf{k}, t)$-space, enabling high spatial resolution by virtue of its extended $\mathbf{k}$-space coverage. Conventionally, readouts of $\mathcal{D}_1$ and $\mathcal{D}_2$ are acquired after separate RF pulses, but other navigation strategies (e.g., self-navigation) are possible.

The temporal subspace $\mathrm{R}(\mathbf{\Phi}^H)$ is typically determined by defining $\mathbf{\Phi}$ from the L most significant right singular vectors of $\mathbf{C}_1$, the Casorati matrix formed from $\mathcal{D}_1$. With $\mathbf{\Phi}$ already determined, the matrix $\mathbf{\Psi}$ with elements $\Psi_{ij} = \psi_j(\mathbf{r}_i)$ is then recovered from $\mathcal{D}_2$ using the subspace constraint $\mathrm{R}(\mathbf{\Phi}^H)$. This can be accomplished through regularized least-squares model fitting:

$$\hat{\mathbf{\Psi}} = \arg\min_{\mathbf{\Psi}} \|\mathbf{d} - \Omega\{\boldsymbol{\mathcal{F}}_{\mathbf{r}}\mathbf{\Psi}\mathbf{\Phi}\}\|^2 + G(\mathbf{\Psi}), \qquad (3)$$

where $\mathbf{d}$ is the measured data, $\Omega\{\cdot\}$ is the sparse sampling operator, $\boldsymbol{\mathcal{F}}_{\mathbf{r}}$ computes the spatial Fourier transform, and $G(\cdot)$ is the regularization function. For the purposes of this paper, we will consider the regularization function from [4]:

$$G(\mathbf{\Psi}) = \lambda_1 \|R\{\mathbf{\Psi}\}\|_{1,2} + \lambda_2 \|\mathrm{vec}(\mathbf{\Psi}\mathbf{\Phi}\boldsymbol{\mathcal{F}}_t)\|_1 , \qquad (4)$$

where $\|R\{\mathbf{\Psi}\}\|_{1,2}$ is a group sparsity penalty that imposes a spatially-varying model order constraint (allowing model order L_1 over the non-cardiac region and model order $L_2 \geq L_1$ over the cardiac region), and $\|\mathrm{vec}(\mathbf{\Psi}\mathbf{\Phi}\boldsymbol{\mathcal{F}}_t)\|_1$ is the spatial-spectral sparsity constraint widely used in compressed sensing cardiac MRI (e.g., [5]–[8]).

III. SELF-NAVIGATION

We propose to perform accelerated T_2^*-weighted cardiovascular MRI through self-navigated explicit-subspace imaging. Our self-navigated method collects readouts of $\mathcal{D}_1$ and $\mathcal{D}_2$ within the space of a single T_R, eliminating the need to expend an entire T_R to collect navigator data. The late $\mathcal{D}_2$ echo time required for T_2^*-weighted imaging leaves room for the navigator signal to be collected prior to each sparse (i.e., $\mathcal{D}_2$) imaging echo, increasing the efficiency of data acquisition. Self-navigation shortens the temporal sampling rate of $\mathcal{D}_1$ from $2T_\mathrm{R}$ to T_R, thereby doubling the frame rate of the final reconstructed images from $1/2T_\mathrm{R}$ to $1/T_\mathrm{R}$.

We accomplish self-navigation by separating the slice rephase, read dephase, and phase encode gradient pulses and collecting navigator data during slice rephasing and read dephasing. The slice rephase and read dephase pulses are the same after every RF pulse, enabling collection of suitable data for $\mathcal{D}_1$. In our implementation, we additionally replace the read dephase pulse with a "music note" (♪) trajectory [9], which has the same integral as the typical read dephase pulse (i.e., it ends in the same $\mathbf{k}$-space location). The 1-D trajectory of the typical read dephase pulse has a null space such that it cannot detect perpendicular translation [9], so it is preferable to use a 2-D navigator such as the music note trajectory or a spiral trajectory. We have designed and implemented the music note to: 1) traverse a high-SNR region of $\mathbf{k}$-space; and 2) be less demanding of gradient hardware than spiral trajectories. We use the same music note navigator trajectory after each RF pulse, but vary the phase encode pulse to acquire different Cartesian imaging readouts of $\mathcal{D}_2$.

Figure 1 shows an example of slice-spoiled FLASH pulse sequences implementing (a) conventional two-pulse navigation and (b) self-navigation. As pictured, our "read dephase" gradient actually traverses the 2-D "music note" trajectory illustrated in Fig. 1-c. Other gradient combinations and $\mathbf{k}$-space trajectories could also be used for self-navigation, but we will consider the implementation represented by Fig. 1-b in the remainder of this paper.

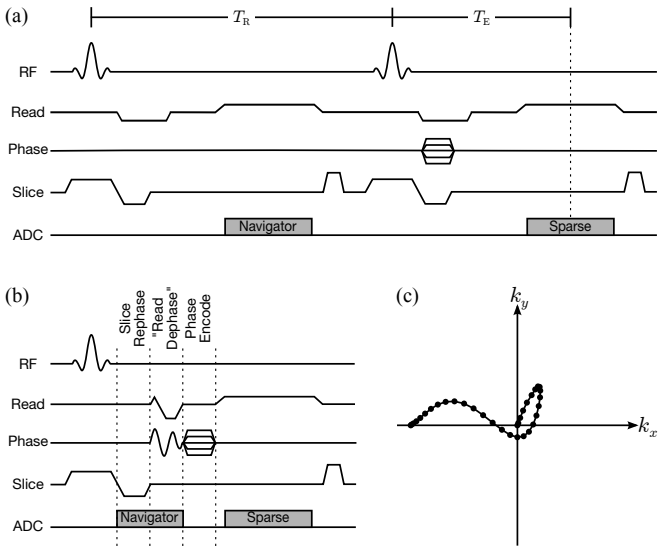

Fig. 1. Slice-spoiled FLASH sequences illustrating (a) the conventional two-pulse navigation strategy, (b) the proposed self-navigated strategy, and (c) the music note trajectory employed in this paper. The self-navigated sequence is half the duration of the conventional sequence, doubling the frame rate of the reconstructed images.

IV. RESULTS AND DISCUSSION

We have evaluated the proposed method in rats by comparing navigator strategies for *in vivo* explicit-subspace imaging using healthy native hearts; we have further evaluated the method for *in vivo* T_2^*-weighted imaging of MPIO-labeled macrophage infiltration using an ischemic reperfusion injury (IRI) model and examined the results against *ex vivo* MRM T_2^*-mapping. *In vivo* scans were performed on a Bruker Avance AV1 4.7 T scanner equipped with a 4-channel array coil. *Ex vivo* scans were performed on a Bruker Avance 11.7 T scanner with a single-channel volume coil. All animals received humane care in compliance with the *Guide for the Care and Use of Laboratory Animals* published by the National Academy of Science [10], and the animal protocol

was approved by the Carnegie Mellon University Institutional Animal Care and Use Committee.

A. Navigation Comparison

To demonstrate the increased speed offered by self-navigation, we have compared navigation strategies for cardiac imaging of healthy Brown Norway (BN) rats. We implemented both customized FLASH pulse sequences shown in Fig. 1: the conventional two-pulse navigation strategy in Fig. 1-a and the music note self-navigation strategy in Fig. 1-b. Imaging data were collected using field of view (FOV) = 40 mm × 40 mm, matrix size = 256 × 256, spatial resolution = 0.16 mm × 0.16 mm, slice thickness = 2 mm, and imaging time = 5 min. Parallel acceleration was performed as in [4] with $N_{\mathrm{ACS}} = 32$ and $P = 2$. Typical timing parameters were T_{R} = 10.5 ms, T_{E} = 5.0 ms, resulting in a frame rate of 48 frames per second (fps) for conventional navigation and a frame rate of 95 fps for self-navigation. All data were collected continually with neither ECG gating/triggering nor breath holding. Images were reconstructed according to [4] using $L_1 = 16$ and $L_2 = 24$, with regularization parameters set according to Morozov's discrepancy principle [11]. Fig. 2 depicts spatiotemporal slices through the heart using (a) conventional navigation, and (b) self-navigation. The self-navigated slice has double the frame rate and is noticeably sharper than that acquired with conventional navigation.

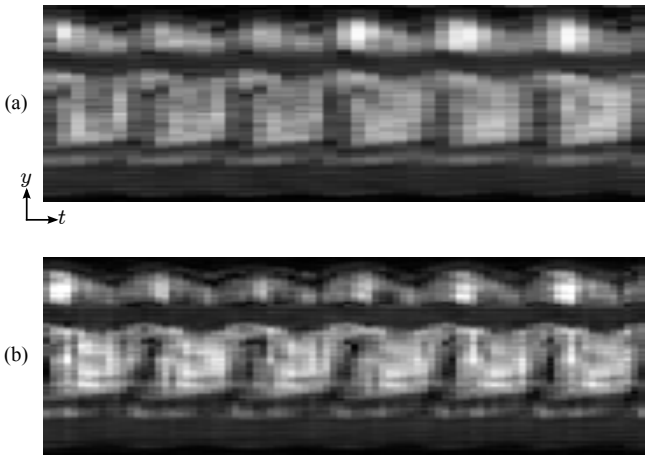

Fig. 2. Spatiotemporal slices over the heart, using (a) conventional navigation at 48 fps and (b) self-navigation at 95 fps. The self-navigated slice is noticeably sharper due to the higher frame rate.

B. MPIO-Labeled Cell Imaging

In order to image infiltration of MPIO-labeled macrophages in the heart, we employed an IRI model using BN rats. IRI was induced by a 45 minute transient occlusion of the left circumflex coronary artery followed by reperfusion, resulting in inflammation of the affected myocardial tissue. Macrophages and monocytes were labeled in circulation by intravenous administration of MPIO particles at least one day before imaging. We evaluated macrophage infiltration *in vivo* through T_2^*-weighted MRI using self-navigated explicit-subspace imaging. To highlight the utility of imaging MPIO-labeled immune cells, we also performed T_1-weighted late gadolinium enhancement (LGE) imaging, which is ubiquitous in cardiac MRI examinations [12]. After the conclusion of *in vivo* imaging, the hearts were excised and fixed in 4% paraformaldehye solution overnight and stored in phosphate buffered saline. T_2^* maps were then obtained using *ex vivo* MRM.

For *in vivo* T_2^*-weighted imaging, data were collected using T_{R} = 10.2 ms, T_{E} = 5.1 ms, field of view (FOV) = 40 mm × 40 mm, matrix size = 256 × 256, spatial resolution = 0.16 mm × 0.16 mm, slice thickness = 1 mm, imaging time = 10 min, $N_{\mathrm{ACS}} = 32$, and $P = 2$. All data were collected continually with neither ECG gating/triggering nor breath holding. Reconstructions were performed as in Section IV-A. The frame rate of the resulting images was 98 fps.

For LGE imaging, the Bruker IntraGate (Bruker BioSpin MRI, Ettlingen, Germany) method was used to acquire retrospectively gated T_1-weighted images 10 minutes after the introduction of a 0.1 mmol/kg bolus of gadolinium-based contrast agent (Gadoteridol). LGE imaging data were collected using T_{R} = 5.6 ms, T_{E} = 3.1 ms, field of view (FOV) = 40 mm × 40 mm, matrix size = 128 × 128, spatial resolution = 0.31 mm × 0.31 mm, slice thickness = 1 mm, and imaging time = 10 min.

Ex vivo scans were performed using a multislice multiecho sequence with T_{R} = 1 s, T_{E} = 8 ms, 16 ms, 24 ms, ..., 64 ms (echoes = 8, echo spacing = 8 ms), FOV = 12.5 mm × 12.5 mm, matrix size =128 × 128, slice thickness = 2 mm.

Fig. 3 shows (a) a self-navigated *in vivo* T_2^*-weighted short-axis slice from a rat with IRI on post-operational day 4, as well as (b) a T_2^* map computed from *ex vivo* MRM. Dark patches are visible in the *in vivo* image and corroborated by the *ex vivo* T_2^* map, indicating macrophage accumulation to the myocardial region affected by the artery ligation. The self-navigated *in vivo* image sequence further revealed myocardial akinesis in the region surrounding the inflamed tissue, consistent with injury to that location.

Fig. 4 shows an LGE image from the same subject as in Fig. 3. The image shows no gadolinium contrast enhancement in the myocardium, indicating that the myocardium is still viable; the only indication of the injury was myocardial akinesis (observed in this image sequence just as in the self-navigated T_2^*-weighted images). The lack of late gadolinium enhancement in Fig. 3 highlights the difference between MPIO-labeled immune cell imaging and LGE imaging, demonstrating the value of imaging macrophage accumulation.

C. Discussion

Fig. 2 reveals the accelerated frame rate provided by self-navigation. The efficiency of the self-navigated pulse sequence offers an immediate two-fold increase in imaging speed without affecting image contrast weighting, thereby enabling high-speed, free-breathing MPIO-labeled cell imaging without ECG or respiratory gating.

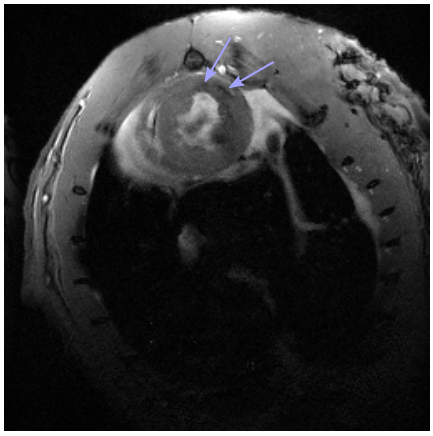

(a)

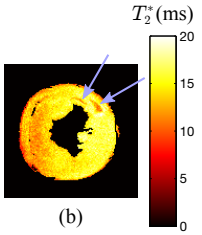

(b)

Fig. 3. MPIO-labeled cell imaging of a short-axis slice on a rat with IRI (post-operational day 4) using (a) self-navigated *in vivo* T_2^*-weighted imaging, and (b) *ex vivo* MRM T_2^*-mapping. The dark patches of myocardial tissue visible in the *in vivo* image indicate macrophage accumulation and are corroborated by the *ex vivo* T_2^* map.

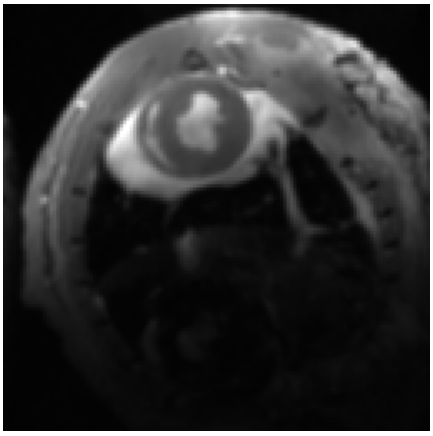

Fig. 4. Gated LGE imaging of the same subject. Despite the reperfusion injury, no gadolinium contrast enhancement is visible in the myocardium, highlighting the difference between MPIO and other contrast mechanisms such as gadolinium-based agents.

Fig. 3 demonstrates the feasibility of self-navigated T_2^* MPIO-labeled cell imaging. The method is capable of producing high-resolution images which indicate macrophage infiltration through negative contrast, allowing noninvasive identification of inflamed tissue. Coupled with the akinesis at the site of the negative contrast (revealed by the *in vivo* images), the high level of agreement between Figs. 3-a and 3-b confirms that the dark patches imaged *in vivo* indeed arise from shortened T_2^* due to the accumulation of MPIO-labeled macrophages.

T_2^*-weighted imaging with SPIO labeling provides complementary information to other contrast weightings and contrast agents, as evidenced by Fig. 4. LGE imaging, which is performed far more commonly than SPIO-labeled cell imaging, is the clinical gold standard for assessing myocardial viability. As such, LGE does not indicate minor injuries which cause inflammation, only injuries that irreversibly damage the myocardium. The lack of gadolinium contrast enhancement in Fig. 4 underscores the utility of SPIO as a contrast agent. Even though the entire myocardium is viable (as demonstrated by the lack of gadolinium contrast enhancement), the tissue is still inflamed, which cannot be inferred from the LGE images alone.

V. CONCLUSION

This work has demonstrated self-navigated low-rank cardiac imaging of inflamed myocardial tissue at 0.16 mm in-plane spatial resolution and 98 fps. The self-navigated method proposed here doubles the imaging speed compared to conventional two-pulse navigation, accelerating MPIO-labeled cell imaging. Using self-navigated T_2^*-weighted imaging, we have observed macrophage accumulation *in vivo* without the use of cardiac or respiratory gating. Our noninvasive method for assessment of MPIO-labeled macrophage accumulation (corroborated by *ex vivo* MRM T_2^* maps and observed regional myocardial akinesis) identified reperfusion injury where gadolinium contrast enhancement could not. Extension of this method to 3-D imaging can potentially provide whole-heart detection of MPIO accumulation, and we believe there is great potential to further develop and apply our methods to perform other inflammatory assessments (e.g., characterization of atherosclerotic plaque). Self-navigation can also accelerate other cardiac imaging applications beyond that explored here.

REFERENCES

[1] Y.-J. L. Wu, Q. Ye, L. M. Foley, T. K. Hitchens, K. Sato, J. B. Williams, and C. Ho, "In situ labeling of immune cells with iron oxide particles: An approach to detect organ rejection by cellular MRI," *Proc. Natl. Acad. Sci. U.S.A.*, vol. 103, pp. 1852–1857, Feb. 2006.

[2] Z.-P. Liang, "Spatiotemporal imaging with partially separable functions," in *Proc. IEEE Int. Symp. Biomed. Imaging*, 2007, pp. 988–991.

[3] J. P. Haldar and Z.-P. Liang, "Spatiotemporal imaging with partially separable functions: A matrix recovery approach," in *Proc. IEEE Int. Symp. Biomed. Imaging*, 2010, pp. 716–719.

[4] A. G. Christodoulou, H. Zhang, B. Zhao, T. K. Hitchens, C. Ho, and Z.-P. Liang, "High-resolution cardiovascular MRI by integrating parallel imaging with low-rank and sparse modeling," *IEEE Trans. Biomed. Eng.*, vol. 60, no. 11, pp. 3083–3092, Nov. 2013.

[5] M. Lustig, J. M. Santos, D. L. Donoho, and J. M. Pauly, "k-t SPARSE: High frame rate dynamic MRI exploiting spatio-temporal sparsity," in *Proc. Int. Soc. Magn. Reson. Med.*, 2006, p. 2420.

[6] U. Gamper, P. Boesiger, and S. Kozerke, "Compressed sensing in dynamic MRI," *Magn. Reson. Med.*, vol. 59, pp. 365–373, Feb. 2008.

[7] H. Jung, K. Sung, K. S. Nayak, E. Y. Kim, and J. C. Ye, "k-t FOCUSS: A general compressed sensing framework for high resolution dynamic MRI," *Magn. Reson. Med.*, vol. 61, pp. 103–116, Jan. 2009.

[8] B. Zhao, J. P. Haldar, A. G. Christodoulou, and Z.-P. Liang, "Image reconstruction from highly undersampled (k, t)-space data with joint partial separability and sparsity constraints," *IEEE Trans. Med. Imaging*, vol. 31, pp. 1809–1820, Sep. 2012.

[9] A. G. Christodoulou, T. K. Hitchens, Y. Wu, C. Ho, and Z.-P. Liang, "Improved subspace estimation for low-rank model-based accelerated cardiac imaging," *IEEE Trans. Biomed. Eng.*, in press.

[10] Committee for the Update of the Guide for the Care and Use of Laboratory Animals; National Research Council, *Guide for the Care and Use of Laboratory Animals: Eighth Edition*. The National Academies Press, 2011.

[11] V. A. Morozov, "On the solution of functional equations by the method of regularization," *Sov. Math. Dokl.*, vol. 7, pp. 414–417, 1966.

[12] P. Kellman and A. E. Arai, "Cardiac imaging techniques for physicians: Late enhancement," *J. Magn. Reson. Imaging*, vol. 36, no. 3, pp. 529–542, 2012.